

# Experimentally Validated Numerical Modeling of Material Deformation across the Scales: A Review

Xu Song, Jonathan P. Belnoue, Felix Hofmann and Alexander M. Korsunsky

**Abstract**—The purpose of the present paper is to provide a brief overview of the recent activities in the Oxford HEX-lab group aimed at the development of experimentally validated deformation models at multiple scales of interest: from macroscopic to meso- to micro-scope level. The emphasis is placed on establishing the connection between the simulation, notably using the Finite Element Method, and the experiment, notably synchrotron x-ray diffraction characterization. The combined approach provides us with a powerful arsenal of analytical tools for the study of deformation behavior of complex materials and engineering components.

**Index Terms**— Oxford HEX-lab, finite element method, coupled local-nonlocal damage plasticity modelling, laser extensometry, eigenstrain method, synchrotron x-ray diffraction, continuum and strain gradient crystal plasticity, energy-dispersive strain measurement and Laue diffraction

## I. INTRODUCTION

Numerical simulation, particularly using Finite Element Methods, has become an indispensable tool serving to underpin scientific investigations of materials deformation and to complement some of the more traditional theoretical approaches. The power of analytical theories lies in their ability to reduce the complex collective behaviour of the basic elements of a solid (e.g. electrons, atoms, lattice defects, and/or single-crystal grains) into insightful relationships between deformation causes and effects. For example, in Finite Element formulations, the description of straining beyond the elastic regime is usually captured by appropriate continuum constitutive equations. The implementation of such relationships within continuum mechanics generally relies on the inherent assumption that material properties vary continuously throughout the solid.

Manuscript received Dec 28, 2011; revised Feb 10, 2012.

Professor Alexander M. Korsunsky is with the Department of Engineering Science, University of Oxford, UK, OX1 3PJ (corresponding author, phone: 0044-18652-73043; fax: 0044-18652-73010; e-mail: [alexander.korsunsky@eng.ox.ac.uk](mailto:alexander.korsunsky@eng.ox.ac.uk)).

Dr Xu Song was doctoral student and Research Associate with the University of Oxford, UK, OX1 3PJ, and is now with the Singapore Institute of Manufacturing Technology, A\* Star, Singapore, 638075 (e-mail: [songx02@gmail.com](mailto:songx02@gmail.com)).

Dr Felix Hofmann was doctoral student and Research Associate with the University of Oxford, UK, OX1 3PJ, and is now in the Chemistry Department, MIT, Cambridge, USA (e-mail: [felix.hofmann.ac@gmail.com](mailto:felix.hofmann.ac@gmail.com)).

Dr Jonathan. P. Belnoue was doctoral student and is now with ACCIS, Department of Aerospace Engineering, University of Bristol, Bristol, UK BS8 1TR (e-mail: [jonathan.belnoue@bristol.ac.uk](mailto:jonathan.belnoue@bristol.ac.uk)).

However, certain heterogeneities linked to either the microstructure or the deformation cannot be readily described within the framework provided by continuum mechanics, i.e. such phenomena as dislocation multiplication and interaction, crack nucleation in fatigue, etc. In the light of the dual nature of the structure of matter (continuous when viewed at coarse length scales, and discrete at finer scales of analysis) and the crucial interdependences between the finer and coarser scales, materials modeling approaches are required to link different scales. On the mesoscopic (or microstructure) scales (in between continuum and atomistic), continuum approaches begin to break down, while atomistic methods reach inherent time and length-scale limitations.

Mesoscopic theoretical frameworks and modeling techniques are being developed that bridge the gap between length-scale boundaries. It is important to note, however, that meaningful development of these refined scale frameworks or “bridging” models only becomes possible when corresponding material deformation characterisation methods become available, such as e.g. laser extensometry, digital image correlation (DIC) and synchrotron X-Ray diffraction. These are employed to probe the material deformation at the corresponding scales, and serve as excellent tools for the determination of crucially important model material parameters needed for the simulation.

This paper presents an overview of the recent advances in multi-scale and experimentally validated modeling conducted within the Oxford HEX-lab group [1,2]. The scope of studies presented spans the range of high-performance alloys, from macroscopic nonlocal damage-plasticity models applied to ductile Al alloys to eigenstrain-based fatigue simulations in light Mg alloys to strain gradient dislocation-based modeling of intragranular deformation in commercially pure Ni.

## II. COUPLED NONLOCAL DAMAGE-PLASTICITY MODELING OF DUCTILE ALLOY PLATES

The growing use of the damage tolerance approach in industry has result in an increasing need for accurate and stable numerical tools able to predict damage and cracks nucleation and propagation in mechanical structures subjected to complex thermo-mechanical loading. For years, engineers had no choice but to use only partially satisfactory FE-based methods whose predictions either couldn't be done without knowing the crack path in advance (i.e. cohesive zone elements, re-meshing techniques, and more

recently XFEM, etc.) or were dependent on the mesh size and orientation (i.e. (local) continuum damage mechanics). Over the past 40 years, simultaneously they were developing the above-mentioned methods researchers started to explore another route now well known as Nonlocal Continuum Damage Mechanics [3]. The method that was first introduced by Pijaudier-Cabot and Bazant [4] uses the general concepts of the (local) Continuum Damage Mechanics theory but the damage-driving state variable (e.g. plastic strain, strain energy release rate, etc..) is replaced by its averaging over a certain volume (see Fig. 1a). This averaging is weighted in order to account for the fact that the further a point is from the central point of the calculation the less influence it is likely to have. This not only has a regularization effect that eases to overcome the numerical instabilities often accompanying damage-induced softening but also corroborates well experimental observations [5] (see Fig. 1b) as it is linked to the material length scale whose existence was proved by many researchers [6,7,8].

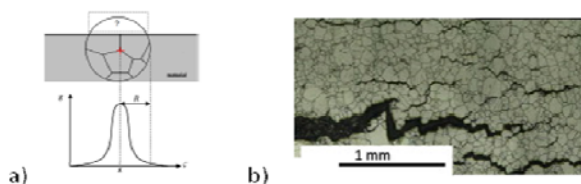


Fig. 1. A) Bell-shaped weight function for nonlocal averaging and its relation to the characteristic length, R. Care must be taken for points in the vicinity of boundaries b) Micrograph of multiple cracks in C263 nickel-base superalloy plate after TMF at 750 °C (nonlocal damage).

Although numbers of nonlocal-type models were proposed from the late 80's, it really only started to be widely accepted by the scientific community 5 or 10 years ago. Even then, however, most of the applications focused on modeling of brittle [9] and quasi brittle materials [10]. Over the past 5 years, researchers of the team have dedicated some efforts in adapting the method to the modeling of ductile metals failure process [11]. The model was derived within the thermodynamical framework proposed by Nguyen [9]. The metal plasticity was described by a Von Mises yield function used in combination with a compounded linear and Chaboche type isotropic hardening law. Using a test material constructed by randomly affecting a value to each of the material parameters needed by the model and an in-house 1D implicit FE program coded in Matlab®, the authors [12] showed the model's ability to overcome numerical instabilities, to give mesh independent results, to debrief of damage-induced size effects and to perform energy work at rupture predictions. The model was then implemented within a user subroutine UMAT for the FE package ABAQUS® [5] and a consistent tangent stiffness matrix was derived [13] in order to achieve good convergence and fast code running. As illustrated in Fig. 2, the model showed good ability to predict crack path in thin plates (plane stress assumption) of relatively complex geometries subjected to pure tensile loading.

One of the most important tasks in material modelling is the identification of the material parameters needed by the

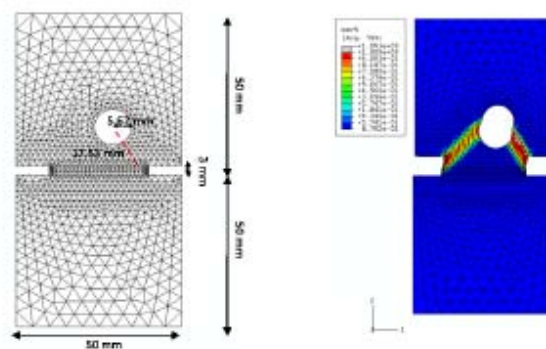


Fig. 2. Nonlocal coupled damage plasticity models are able to predict crack path in thin plates made of ductile metal alloys and subjected to pure tensile loading. As shown on the right hand side picture, which illustrates the damage distribution at the end of the failure process in the plate whose geometry is given on the left hand side picture, a crack is represented by a band of fully damaged material.

model. If a nonlocal damage-plasticity model is used, the level of complexity of this operation drastically increases. This is due to the coupling between plasticity and damage as much as to the dependence of the response on the material length scale. Therefore the parameter identification procedure has to be made against experimental data containing information on the material length scale. Successful calibration methods of nonlocal damage plasticity models often necessitates to perform series of tests on specimens of different sizes but of similar geometries and to use computationally-demanding parameter identifications procedures (such as Markovian optimization, least squares fitting, Levenberg-Marquardt algorithm, etc.) able to solve strongly coupled inverse problems. With the aim to ease the procedure, the authors set up a new linked experimental and modelling approach, whereby a single tensile test is used, with multiple gauge length extensometry, to obtain the information about material size effects; an adaptive calibration procedure (see in [14]) for the damage function is applied to match the experimental data. Bifurcation analysis of the model also showed that the determination of the nonlocal radius can be accomplished readily on the basis of the same set of experimental data (i.e. the nonlocal radius is essentially equal to the size of the

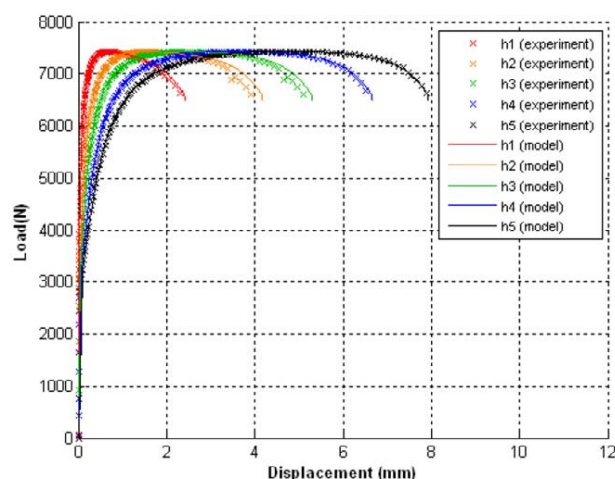


Fig. 3: Load-extension curves of a 3 mm-thick dog-bone specimen in aluminium AA6082 T0 obtained for sub-specimen of initial lengths:  $h_1=23$  mm,  $h_2=17$  mm,  $h_3=11$  mm,  $h_4=7$  mm, and  $h_5=3$  mm. Model predictions are superimposed on experimental data.

strain localization area experimentally observed). Figure 3 illustrates the quality of the resulting calibration. The load-extension curves for all the sub-specimens considered are captured equally well, indicating that the size effect and the energetic characteristics of the plastic rupture process are adequately represented by the model. Crack nucleation and propagation can be captured well by nonlocal continuum damage mechanics models. Full-field measurements techniques such as laser extensometry or DIC allow a relatively easy determination of the great number of material parameters required. However, the presence and effect of the residual stresses, is not accounted for in this model.

### III. AN EIGENSTRAIN-BASED CONTINUUM PLASTICITY MODEL IN STUDYING THE EVOLUTION OF RESIDUAL STRESSES DURING LOW CYCLE FATIGUE

To understand the effect and evolution of residual stresses in the structural materials during Low Cycle Fatigue (LCF) is an enduring objective of the engineering community. In this case, the evolution of shot peening induced residual stresses in GW103 (Mg-Gd-Y) alloy during LCF is studied by using the inverse eigenstrain method to incorporate residual stresses into finite element simulation [15]. The inverse eigenstrain method was firstly introduced by Korsunsky et al. [16] with the piecewise linear description of the inelastic strain distribution in either 1D [17] or 2D [18] obtained by the minimization of the difference between the residual stresses obtained from an FE model and the experimental data.

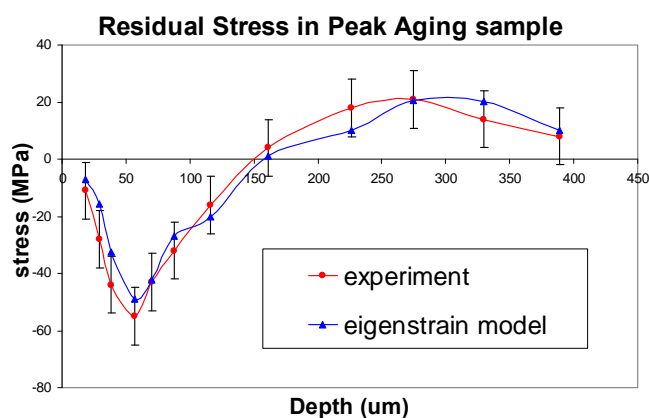


Fig. 4. Residual stress profiles in the peak-aged sample with optimal Almen intensity and eigenstrain model approximation.

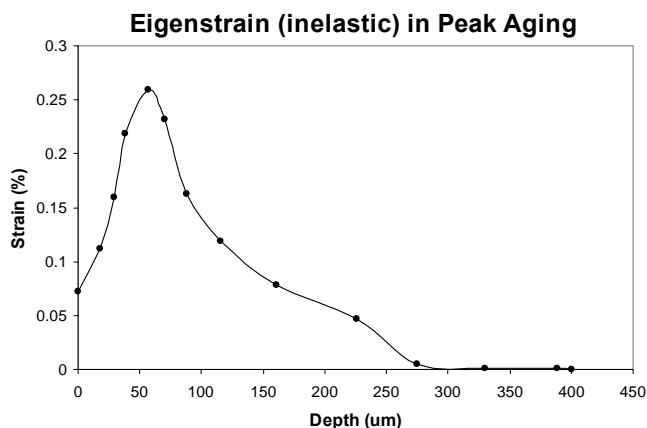


Fig. 5. Reconstructed eigenstrain (plastic strain) in peak-aged sample due to shot peening.

The minimization procedure can be readily implemented in ABAQUS™ via model pre- and post- processing [18]. In this way the “most likely” distribution of eigenstrain (in our case, plastic strain) is obtained within the shot-peened sample based on the knowledge of the residual stress distribution. From Fig. 4, we can tell that the reconstructed residual stresses showed good agreement with the experimental data. Hence, the plastic strain distribution within the sample was, as reconstructed, plotted in Fig. 5. In order to have a better understanding and a more compact description of the eigenstrain distribution, a concise and easy-to-implement functional expression for the eigenstrain profile is proposed here in (1). This function is a sum of two Gaussian peaks with different central positions and widths:

$$\varepsilon^*(x) = A_1 \exp\left(-\frac{(x-\mu_1)^2}{2\sigma_1^2}\right) + A_2 \exp\left(-\frac{(x-\mu_2)^2}{2\sigma_2^2}\right) \quad (1)$$

The parameters found by least square fitting for the peak-aged sample were:  $A_1=0.19$  (%),  $A_2=0.08$  (%),  $\mu_1=55$  ( $\mu\text{m}$ ),  $\mu_2=110$  ( $\mu\text{m}$ ),  $\sigma_1=30$  ( $\mu\text{m}$ ),  $\sigma_2=100$  ( $\mu\text{m}$ ). This description captures not only the primary plastic strain peak which creates the maximum compressive residual stress in the sample, but also the “hump” behind it that controls the plastic strain penetration depth (see Fig. 6). By employing this function, the plastic strain and the residual stress state created by shot peening can be readily incorporated in the FE model as the initial step of the simulation using the eigenstrain method.

The next stage in our simulation of the shot peening

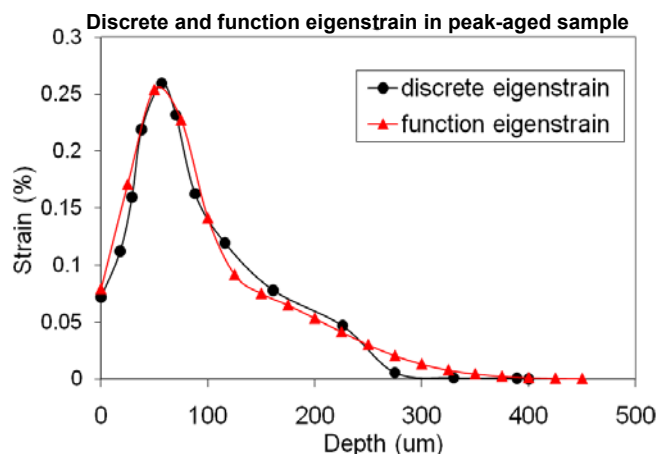


Fig. 6. Comparison between the discrete eigenstrain reconstruction plastic strain profile and the functional description.

residual stress evolution is to consider the unknown material hardening history that is experienced by the sample surface. The hardening history is important to our modelling approach, because the plastic strain created by shot peening is accompanied by material hardening that modifies the shape and extent of the yield surface in the stress space. This effect is not accounted for in the simple eigenstrain reconstruction, but may in fact have a significant impact on the material behaviour during subsequent loading [19, 20]. A novel approach is proposed here which can be used to capture this history-dependent hardening effect. First, a parameter-based hardening continuum plasticity model is chosen and implemented in ABAQUS™ using the user subroutine UMAT. The general framework was proposed

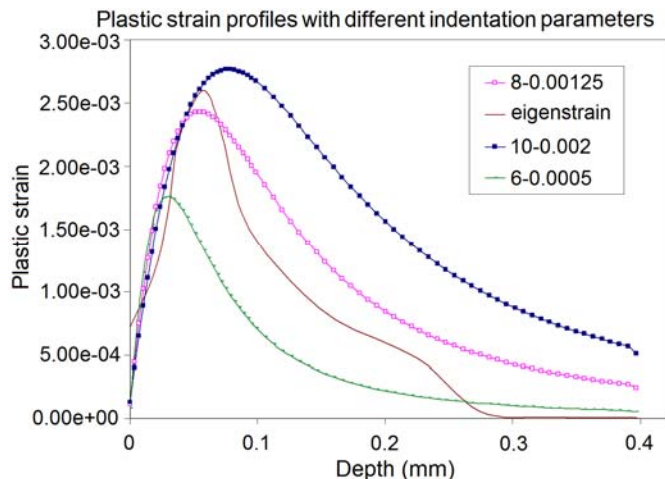


Fig. 7. Optimization of the indentation parameters against the eigenstrain profile, three representative parameter combinations are plotted.

by Mahnken [21] with isotropic hardening stress of Chaboche type [22] augmented by a linear evolution term, and a kinematic hardening term of Armstrong and Frederick type [22], where  $c, b, h, k_1, k_2$  are the material parameters to be calibrated against experimental LCF data. This calibration exercise returned the parameter values of  $c=0$  MPa,  $b=0$ ,  $h=0$  MPa,  $k_1=5300$  MPa and  $k_2=45$  MPa, which is essentially a kinematic hardening condition. The next challenge was to relate the plastic strain (eigenstrain) with the back stresses created by shot peening, so that the hardening history was captured. This was achieved by considering spherical indentation as representative of the elementary act involved in the shot peening treatment. The aim of the Finite Element simulation of the elasto-plastic indentation by a rigid spherical punch is to develop a prediction of the depth-varying mechanical states. More specifically, two aspects were sought: (i) the distribution of eigenstrain (and hence residual stress), and (ii) the distribution of the material hardening parameters (combined kinematic and isotropic description). By choosing the right combination of indenter radius and depth, the best approximation to the eigenstrain profile was found (Fig. 7), in which the back stress and plastic strain component perpendicular to the indentation direction follow a simple linear relationship:

$$\mathbf{X} = \mathbf{k}\boldsymbol{\epsilon}_{xx}^{pl} \quad (2)$$

This remarkably simple (but accurate) result allows us to link the experimentally found eigenstrain (plastic strain) distribution to the ‘initial’ back stresses. We have thus derived a way of incorporating the effect of the material hardening history during shot peening in the simulation of subsequent sample deformation.

In the present study, this residual stress evolution phenomenon was studied by synchrotron X-ray diffraction in the experiment carried out on beamline ID15B at the ESRF (Grenoble, France). A monochromatic 2-D diffraction set-up was used to collect diffraction patterns (Fig. 8). The diffraction patterns (Debye-Scherrer rings) registered by the detector were analysed using Fit2D via the procedures of "caking" and binning to obtain the equivalent 1-D profiles [23, 24]. Then Rietveld refinement [25] was carried out on the binned 1-D diffraction patterns using GSAS (General

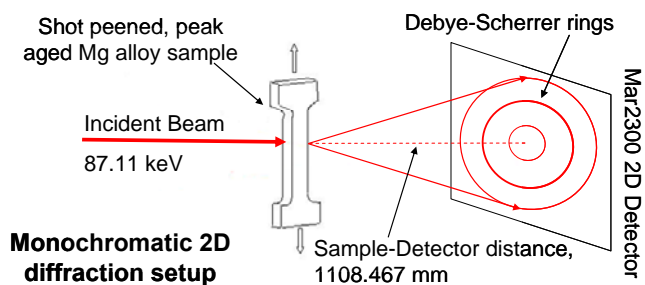


Fig. 8. Monochromatic 2D polycrystalline diffraction setup in ID15B, ESRF for residual stresses measurement in shot peened peak-aged GW103 sample

Structure Analysis System) software to determine the apparent value of the lattice parameter within each gauge volume. The shot-peened, peak-aged sample was then subjected to in situ step loading during X-ray diffraction data collection. The residual elastic strain profiles for the loading steps of 0%, 0.3%, 1.8%, 3.5% and 5.9% (total strain) were collected, and are plotted in Fig. 9.

It is clear from Fig. 9 that at around 0.3% of total strain,

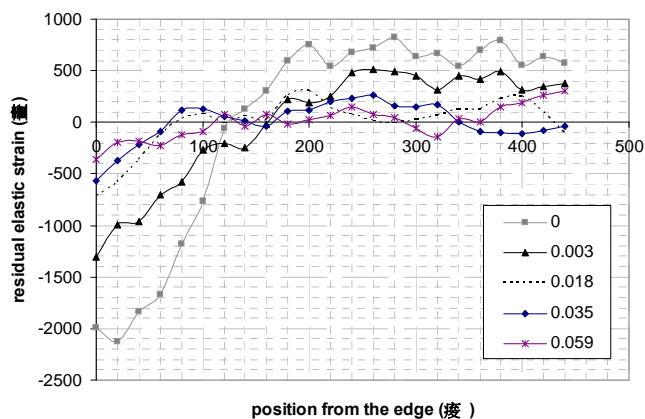


Fig. 9. The evolution of residual strain of the shot peened peak-aged sample. The legend shows the values of total applied strain.

the residual stresses within the sample already show a dramatic decrease from the original values seen at the first loading increment. At a strain of 1.8%, the residual stress profile flattens out, with the maximum value not exceeding 500  $\mu\epsilon$ . The ‘‘peak’’ near the sample surface created by shot peening completely disappears at this stage. For strain levels between 3.5% and 5.9% or higher, the residual strain magnitudes remain almost unchanged, implying that the plastic strain introduced by shot peening has been ‘washed

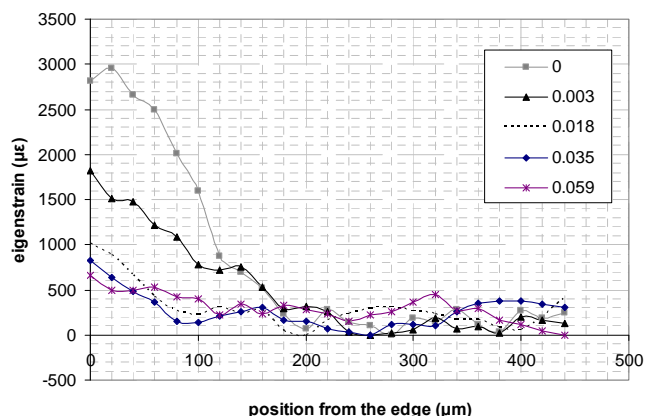


Fig. 10. The evolution of eigenstrain of the shot peened peak-aged sample. The legend shows the values of total applied strain.

out' by the overwhelming plastic deformation in the LCF process. This claim is further corroborated by the eigenstrain profiles extracted from Fig. 9, which have been plotted in a separate graph in Fig. 10.

The experimental observations and the interpretation of residual stresses evolution in the shot-peened, peak-aged GW103 sample can be explained using our eigenstrain model. Fig. 11 illustrates our prediction for the evolution of plastic strain under compressive loading following shot peening. It is apparent that the shot-peening-induced plastic strain remains unchanged until the total compressive strain reaches the level of about 0.33%. This demonstrates the existence of a threshold value of tensile strain that must be applied before residual stress shake-down begins under LCF conditions. This can be expected to be the case for both tensile and compressive loading, albeit with different threshold strain values. Note that the above threshold value is significantly smaller than the monotonic (nominal) yield strain of  $\sim 0.55\%$ . This is the result of the compressive residual stress combining with the applied compressive stress so that yielding occurs sooner. The non-uniform plastic strain distribution after shot peening changes due to plastic straining under compressive loading, and disappears entirely after 1% total strain (equivalent to 0.45% applied plastic strain). This explains why in the experiment at 1.8% strain the residual stress profile became flat. This was due to the gradual elimination of the eigenstrain distribution inherited from the shot peening process.

The experimental observations and numerical modelling combine to support the conclusion that residual stress evolution under LCF conditions can be captured by monitoring the eigenstrain variation due to applied loading.

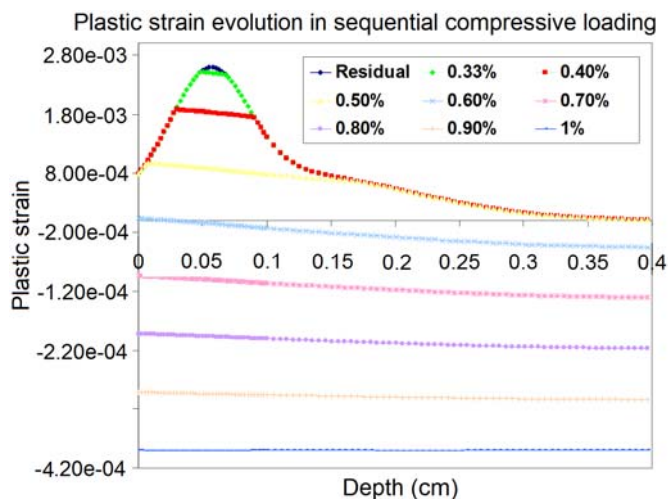


Fig. 11. The evolution of plastic strain under compression of the peened peak-aged sample. The legend shows the values of total applied compressive strain.

#### IV. PROBING LOCAL LATTICE MISORIENTATION BY STRAIN GRADIENT CRYSTAL PLASTICITY MODELLING AND MICRO-BEAM LAUE DIFFRACTION EXPERIMENT

The deformation behaviour of polycrystalline materials in engineering components is crucial to their performance in service. However, it does not occur uniformly in constituent

grains, but shows strong inter- and intra-granular variations at the meso- to microscopic level. These are caused by lattice rotation/misorientation, anisotropic elastic-plastic properties and differences in the damage behaviour, etc. Conventional continuum mechanics as mentioned above does not account correctly for the factors of complex grain shape and intra-granular strain variation at the characteristic length scales of dislocation distributions. Hence, strain gradient crystal plasticity theory [6] was proposed to capture the local inhomogeneity and the length-scale-dependent strengthening effect, based on the development of the concept of Geometrically Necessary Dislocations (GNDs) [6, 26]. An explicit and succinct relationship between shear strain gradients and GNDs was found [26] and generalized [27]. To obtain the information about the meso- to microscopic variations of elastic strains and stresses experimentally, micro-beam Laue diffraction technique was employed due to its suitable spatial resolution. Sharp micron-sized white X-ray beams can probe the deformation and crystal structure (including orientation) at the meso- to microscopic level [28]. By analyzing Laue diffraction spot locations and shapes, it is possible to obtain crystallographic information for the illuminated area, i.e. the local lattice rotation and misorientation, deviatoric strain, etc. It is also possible to predict the Laue spot shapes from known dislocation distributions, which is the objective of this work.

In order to capture the inter- and intra-granular deformation, a realistic representation of the material's microstructure is achieved here with a detailed "replica" of the scanned area characterised by micro-beam Laue diffraction. The grain orientations were found from the analysis of Laue patterns using XMAS [29], and the entire microstructure was then implemented into a grain-based FE mesh. The scan area was  $4 \times 2 \text{ mm}$ , with both the beam size and step size of  $50 \mu\text{m}$ . The sample studied in the experiment was made from commercially pure Ni with FCC crystal structure having a total of 12  $\{111\} \langle 110 \rangle$  slip systems. To visualize the grain morphology and orientation, Schmid

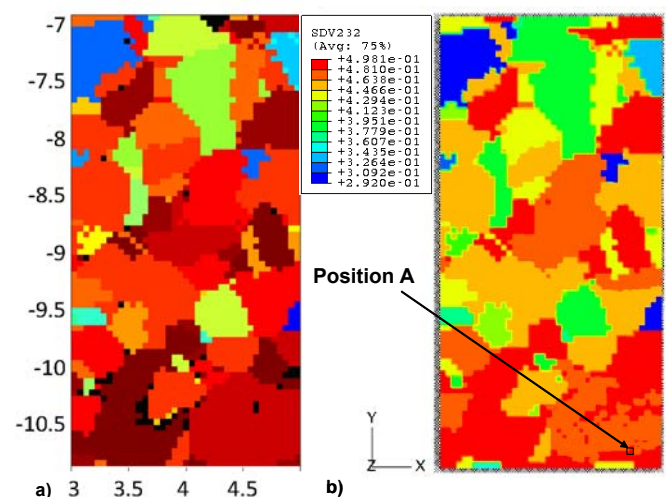


Fig. 12. (a) Schmid factor map (to Y-axis/loading direction) of the Ni sample scanned area analyzed by XMAS (b) Schmid factor map in FE model with selected position A.

factor colour maps are plotted in Fig. 12.

The present model has been implemented by the authors on the basis of the lengthscale-dependent, rate-dependent formulation [30]. The formulation is built on the expression

for the shear strain rate on a particular slip system  $\alpha$ . This shearing rate is thermally dependent via a Boltzmann type exponential thermal activation expression, and also contains a dependence on the system-specific critical resolved shear stress (slip resistance)

$$\dot{\gamma}^\alpha = \dot{\gamma}_0 \exp\left[-\frac{F_0}{k\theta} \left\{1 - \left\langle \frac{|\tau^\alpha| - S^\alpha \mu / \mu_0}{\hat{\epsilon}_0 \mu / \mu_0} \right\rangle^p \right\}^q\right] \quad (3)$$

The central element of the present length scale dependent, dislocation-based deformation modeling approach is the system of evolution laws for the densities of edge and screw types of Statistically Stored Dislocations (SSD) and three types of Geometrically Necessary Dislocations (GND) and their contribution to the slip resistances on the corresponding planes. It is, specifically, the GND contribution that is closely linked to plastic strain gradient effects, and thus causes size and scale dependent effects. The formulation is fully implicit, with its highlight on introducing a special shape function for internal Gauss points of the quadratic element to obtain the spatial derivatives of the plastic deformation gradient.

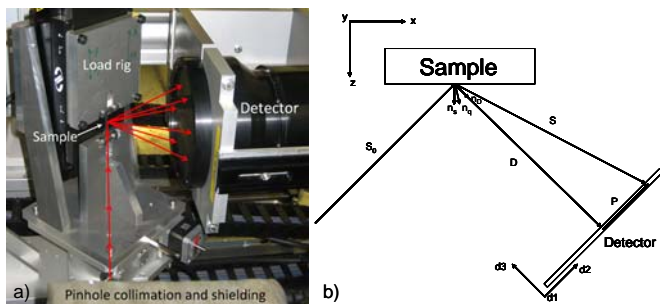


Fig. 13. (a) 90° reflection Laue setup at beamline B16, Diamond Light Source; (b) Illustration of the setup for 90° reflection Laue experiment.

Diffraction experiments were carried out on beamline B16, Diamond Light Source. The incident beam was “pink” with an energy range 5-25keV. The 90° reflection Laue setup was employed [31] (Fig. 13a). The geometric parameters of the setup were accurately determined through calibration shots collected from a Si wafer sample before the Ni sample was mounted. The sample was in-situ loaded, while Laue patterns were collected at different loading stages. The 90° reflection Laue setup is conceptualized in the model using a succinct vector space expression [32] (Fig. 13b). Based on which, a forward prediction post-processor was developed to extract the elastic rotation matrix from each IP in the model and calculates the Laue spot positions on the detector. The resulting spot is obtained by the superposition of the reflections from each IP. Fig. 14(a) shows an experimental Laue pattern from the sample position A (Fig. 12b) under 2% plastic strain. The SGCP model under the same amount of deformation was post-processed to generate the simulated diffraction pattern shown in Fig. 14b. It is generally believed [33] that the change in Laue spot positions is due to the combined effect of lattice rigid body rotation and deviatoric strain; the change of Laue spot shape is due to the local lattice curvature. Notably, the “streaking” (elongation) phenomenon of the Laue spots is due to the presence of GNDs, which are related to the plasticity-induced local lattice misorientation. Figs. 14a and 14b show reasonable

agreement with each other in terms of the spot positions, indicating that the model captures correctly some features of the elasto-plastic deformation, particularly the rigid body rotation and deviatoric strain. A closer look at the spot shapes of reflection 006 from simulation (Fig. 14d) and experiment (Fig. 14c) shows satisfactory agreement in terms of streaking direction and length, indicating the correct prediction of local lattice misorientation, or to say, quantities

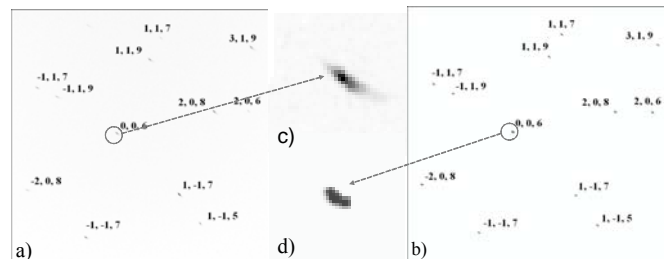


Fig. 14. (a) Experimental Laue diffraction pattern from 2% plastically deformed Ni at position A; (b) Simulated Laue pattern from SGCP model; (c) “Streaking” of the Laue spot (006) in the experiment; (d) “Streaking” of the Laue spot (006) in the simulation

of mixed types of GNDs [33].

## V. CONCLUSION

Finite element simulations were tightly coupled to material deformation characterization methods such as synchrotron x-ray diffraction, laser extensometry and digital image correlation (DIC). This coupling provided us with invaluable tools for investigating material deformation at different scales, and refining advanced constitutive models. With the advance of computer power and analytical techniques, the combined approach of numerical simulation and experimental characterization is set to become the mainstream of material behaviour studies.

## REFERENCES

- [1] A.M. Korsunsky, S.Y. Zhang, D. Dini, W.J.J. Vorster, J. Liu, “Oxford HEXameter: Laboratory high energy X-ray diffractometer for bulk residual stress analysis”, *Mat. Sci. Forum.*, Vol. 524-525, pp.743-748, 2006
- [2] A.M. Korsunsky, F. Hofmann, X. Song, S. Eve, and S.P. Collins, “Probing Deformation Substructure by Synchrotron X-ray Diffraction and Dislocation Dynamics Modelling”, *J. Nanosci. Nanotechnol.*, Vol. 10, pp. 5935-5950, 2010
- [3] Z.P. Bazant and M. Jirasek, “Nonlocal Integral Formulations of Plasticity and Damage: Survey of Progress,” *J. Eng. Mech.*, Vol. 128, pp. 1119-1149, 2002
- [4] G. Pijaudier-Cabot and Z.P. Bazant, “Nonlocal Damage Theory,” *J. Eng. Mech.*, Vol. 113, pp. 1512-1533, 1987
- [5] J.P. Belnoue, B. Garnham, M. Bache and A.M. Korsunsky, “The use of coupled nonlocal damage-plasticity to predict crack growth in ductile metal plates,” *Eng Frac Mech.*, 77, pp. 1721-1729, 2010
- [6] N.A. Fleck, G.M. Muller, M.F. Ashby, and J.W. Hutchinson, “Strain Gradient Plasticity: Theory and Experiment,” *Acta Metallurgica et Materialia*, Vol. 42, pp. 475-487, 1994
- [7] W.J. Poole, M.F. Ashby, and N.A. Fleck, “Micro-Hardness of Annealed and Work-Hardened Copper Polycrystals,” *Scripta Materiala*, Vol. 34, pp. 559-564, 1996
- [8] A.M. Korsunsky and K. Kim, “Determination of essential work of necking and tearing from a single tensile test,” *Int. J. Fract.*, Vol. 132, pp. 37-34, 2005
- [9] G.D. Nguyen, “A thermodynamic approach to constitutive modelling of concrete using damage mechanics and plasticity theory,” D.Phil. Thesis, Dept. of Engng. Sci., University of Oxford, 2005
- [10] R.H.J. Peerlings, R. de Borst, W.A.M. Brekelmans, J.H.P. de Vree, “Gradient-enhanced damage for quasi-brittle materials,” *Int. J. Numer. Meth. Engrg.*, Vol. 39, pp. 3391-3403, 1996

- [11] J.P. Belnoue, "Local-Nonlocal Coupled Damage-Plasticity Modelling of Ductile Materials," D.Phil. Thesis, Dept. of Engng. Sci., University of Oxford, 2010
- [12] J.P. Belnoue, G.D. Nguyen, and A.M. Korsunsky, "A One-Dimensional Nonlocal Damage-Plasticity Model for Ductile Materials," *Int. J. Fract.*, Vol. 144, pp. 53-60, 2007
- [13] J.P. Belnoue, G.D. Nguyen, and A.M. Korsunsky, "Consistent tangent stiffness for local-nonlocal damage modelling of metals," *Procedia Engineering*, Vol 1, pp. 177-180, 2009
- [14] J.P. Belnoue and A.M. Korsunsky, "A damage function formulation for nonlocal coupled damage-plasticity model of ductile metal alloys," *European Journal of Mechanics / A Solids, In Press*, 2011
- [15] X. Song, W.C. Liu, J.P. Belnoue, J. Dong, G.H. Wu, W.J. Ding, S.A.J. Kimber, T. Buslaps, A.J.G. Lunt and A.M. Korsunsky, "An eigenstrain-based finite element model and the evolution of shot peening residual stresses during fatigue of GW103 magnesium alloy (Periodical style—Accepted for publication)," *Int. J. Fatigue*, to be published.
- [16] A.M. Korsunsky, G.M. Regino and D. Nowell, "Variational eigenstrain analysis of residual stresses in a welded plate," *Int. J. Solids. Struct.* Vol. 44 pp.4574–4591, 2006.
- [17] X. Song, S. Chardonnet, G. Savini, S.Y. Zhang, W.J.J. Vorster and A.M. Korsunsky, "Experimental / modelling study of residual stress in Al/SiCp bent bars by synchrotron XRD and slitting eigenstrain methods," *Mater. Sci. Forum.*, Vol. 571–572 pp. 277–282, 2007.
- [18] X. Song and A.M. Korsunsky, Fully two-dimensional discrete inverse eigenstrain analysis of residual stresses in a rail head, *J. Appl. Mech. Trans. ASME*, 78 (2011) art. no. 031019.
- [19] S.A. Meguid, G. Shagal, J.C. Stranart, J. Daly, "Three-dimensional dynamic finite element analysis of shot-peening induced residual stresses," *Finite. Elem. Anal. Des.* Vol. 31 pp.179-191, 1999.
- [20] J.L. Chaboche and O. Jung, "Application of a kinematic hardening viscoplasticity model with thresholds to the residual stress relaxation," *Int. J. Plasticity*, Vol. 13 pp. 785-807, 1998.
- [21] R. Mahnken, "Improved implementation of an algorithm for non-linear isotropic/kinematic hardening in elastoplasticity," *Commun. Numer. Meth. Engng.* Vol. 15 pp. 745-754, 1999.
- [22] J. Lemaitre, J.L. Chaboche, *Mechanics of Materials* (Book style) Cambridge: Cambridge University Press, 1990.
- [23] A.M. Korsunsky, K.E. Wells, P.J. Withers, "Mapping two-dimensional state of strain using synchrotron X-ray diffraction." *Scripta. Mater.* Vol. 39 pp. 1705-1712, 1998.
- [24] A.M. Korsunsky, N. Baimpas, X. Song, J. Belnoue, F. Hofmann, B. Abbey, M. Xie, J. Andrieux, T. Buslaps, T.K. Neo, "Strain tomography of polycrystalline zirconia dental prostheses by synchrotron X-ray diffraction," *Acta. Mater.* Vol. 59 pp. 2501-2513, 2011.
- [25] M.R. Daymond, M.A.M. Bourke, R.B. Von Dreele, B. Clausen, T. Lorentzen, "Use of Rietveld refinement for elastic macrostrain determination and for evaluation of plastic strain history from diffraction spectra," *J. Appl. Phys.* Vol. 82 pp. 1554-1562, 1997.
- [26] M.F. Ashby, "The deformation of plastically non-homogeneous materials," *Phil. Mag.*, Vol. 21, pp. 399-424, 1970.
- [27] E.P. Busso, F.T. Meissonnier and N.P. O'Dowd, "Gradient-dependent deformation of two-phase single crystals," *J. Mech. Phys. Solids*, Vol. 48, pp. 2333-2361, 2000.
- [28] N. Tamura, A.A. MacDowell, R.S. Celestre, H.A. Padmore, B. Valek, J.C. Bravman, R. Spolenak, W.L. Brown, T. Marieb, H. Fujimoto, B.W. Batterman and J.R. Patel "High spatial resolution grain orientation and strain mapping in thin films using polychromatic submicron x-ray diffraction," *Appl. Phys. Lett.*, Vol. 80, pp. 3724-3726, 2002.
- [29] N. Tamura, (1997) XMAS (X-ray Microdiffraction Analysis Software), [http://xraysweb.lbl.gov/microdif/user\\_resources.htm](http://xraysweb.lbl.gov/microdif/user_resources.htm)
- [30] K.S. Cheong and E.P. Busso "Discrete dislocation density modelling of single phase FCC polycrystal aggregates," *Acta Mater.*, Vol. 52, pp. 5665-5675, 2004.
- [31] F. Hofmann, X. Song, I. Dolbnya, B. Abbey and A.M. Korsunsky, "Probing intragranular deformation by micro beam Laue diffraction," *Proc. Eng.*, Vol. 1, pp. 193-197, 2009.
- [32] X. Song, F. Hofmann and A.M. Korsunsky "Dislocation-based plasticity model and micro-beam Laue diffraction analysis of polycrystalline Ni foil: a forward prediction," *Phil. Mag.*, Vol. 90, pp. 3999-4011, 2010.
- [33] R.I. Barabash, G.E. Ice, B.C. Larson, G.M. Pharr, K.S. Chung and W. Yang, "White microbeam diffraction from distorted crystals," *Appl. Phys. Lett.*, Vol. 79, pp. 749-751, 2001.